RSC Advances

ROYAL SOCIETY OF CHEMISTRY

www.rsc.org/advances

Journal Name

ARTICLE

Controlled covalent binding of antiferromagnetic tetramanganese complexes to carbon nanotubes

Received 00th January 20xx,
Accepted 00th January 20xx

DOI: 10.1039/x0xx00000x

www.rsc.org/

R. Frielinghaus,‡[a] C. Besson,‡[b] L. Houben,[c] A.-K. Saelhoff,[a] C. M. Schneider[a] and C.Meyer*[a]

We report on covalent functionalization of carbon nanotubes with tetreamanganese complexes. The process is based on ligand exchange with carboxylic groups on the preliminarily oxidized tubes and does not fundamentally affect the antiferromagnetic coupling between the manganese ions of the complex. We present detailed analysis of the oxidation process and demonstrate that the degree of functionalization directly relates to the density of carboxylic groups. The coverage of a carbon nanotube can be decreased enough to enable fabrication of electronic devices incorporating an individual molecule.

Introduction

Molecular electronics and spintronics concern themselves with the study of transport of electron charges and spins along molecular systems, with expected applications as diverse as the construction of ultra-sensitive sensors,[1, 2] the miniaturization of electronic devices [3-5] including spin as additional degree of freedom for information processing,[6] and the creation of quantum bits for the construction of quantum computers.[7-10] The first requisite for the assembling of a molecular electronics or spintronics device is the reliable connection of the molecule of interest to an electrode system. While numerous studies have described the behaviour of molecules deposited in the gap formed between two metallic electrodes by electromigration or a break junction process,[11, 12] the direct flow of electrons through a molecule alters its properties. In particular, magnetic properties change with the oxidation state.[13] An alternative is offered by the use of carbon nanotubes. With their excellent conductivity, a diameter of only a few nanometres and a length that can routinely reach several micrometres, single-wall carbon nanotubes represent an ideal contacting material bridging between the molecular and the macroscopic scales.[14] Additionally, the long spin-flip lengths and spin lifetimes permitted by the low spin-orbit coupling and few nuclear spins in carbon atoms is a significant advantage with respect to spintronics applications. Among the various functionalization methods[15-17] available for carbon nanotubes (Van der Waals adsorption,[18, 19] electrostatic interaction,[20] direct functionalization of the carbon nanotube wall[21, 22]), we selected ligand exchange between our precursor metal complex $[Mn^{II}_4(OAc)_4L_2]$ (H_2L=2,6-*bis*(1-(2-hydroxyphenyl)iminoethyl)pyridine) and carboxylate functions present on oxidized nanotubes so as to obtain the shortest possible link between the spintronics-relevant magnetic centres of the complex and the conducting carbon nanotube. Besides the presence of labile carboxylate ligands,[23] the targeted complex presents the additional advantage of a diamagnetic ground state due to the predominantly antiferromagnetic coupling between the $S = 5/2$ Mn^{II} centres, thus ensuring a minimal dipole-dipole interaction between neighbouring complexes along the carbon nanotubes. We recently briefly reported on the effectiveness of the binding reaction.[24] Here, we expand on these results and demonstrate control of the density of functionalization of the nanotube as well as of the magnetic properties of the attached complex, two prerequisites for the application of the system in a spintronics setting.

Experimental

Materials and methods

Bulk single-wall carbon nanotubes (90% nominal purity, 1-2 nm diameter, mixed chirality) were purchased from Arry Germany GmbH and further purified by oxidative treatment and base wash (see below). All other starting materials were used as received. Complex $[Mn_4L_2(OAc)_4]$ (H_2L = 2,6-*bis*(1-(2-hydroxyphenyl)iminoethyl)pyridine) was synthetized according to the literature.[23] Thermogravimetric analysis was performed using a using a Mettler-Toledo TGA/SDTA 851e instrument with a heating rate of 10 $K.min^{-1}$. CHN analysis was performed by combustion in a vario EL cube (elementar). For the determination of manganese content, a carbon nanotube

[a] Peter Grünberg Institute (PGI-6), Forschungszentrum Jülich, 52425 Jülich, Germany and JARA-Fundamentals of Future Information Technologies, Germany. E-mail: c.meyer@fz-juelich.de
[b] Institute of Inorganic Chemistry, RWTH Aachen University, Aachen, Germany and JARA-Fundamentals of Future Information Technologies, Germany.
[c] Peter Grünberg Institute (PGI-5) and Ernst Ruska-Centre for Microscopy and Spectroscopy with Electrons, Forschungszentrum Jülich, 52425 Jülich, Germany.
† Electronic Supplementary Information (ESI) available: Direct correspondence between HAADF and EELS data. HAADF images of various sites of the sample with t_{ox} = 2 min. EDS of the sample with t_{ox} = 30 min. See DOI: 10.1039/x0xx00000x
‡ These authors contributed equally to this work.

sample (10-20 mg) was first mixed with lithium metaborate (250 mg) and heated for 30 min to ca. 1050°C in a Pt/Au crucible in a muffle furnace, then the resulting melt was dissolved in 5 % HCl (30 mL), the solution diluted to 50 mL and its manganese content determined by inductively coupled plasma optical emission spectrometry (ICP-OES). Scanning transmission electron microscopy (STEM) in high angle annular dark field mode (HAADF), and electron energy loss spectroscopy (EELS) were performed using a probe-corrected FEI Titan 80-300 microscope operated at 300 kV. An FEI Titan 60-300 microscope equipped with a CEOS achroplanator for chromatic and spherical aberration correction ("PICO") was used for bright field and energy filtered imaging at an acceleration voltage of 80 kV. Energy filtered images were taken using an energy window of 20 eV around the Mn-L23 core-loss excitation with the background extrapolation from five pre-edge measurements. Magnetic measurements were performed using a Quantum Design MPMS XL SQUID magnetometer equipped with the reciprocal sample option. The samples were held in a gelatine capsule mounted in a plastic straw. The diamagnetic contribution of the manganese complex was measured using the zinc analogue and subtracted from the data.

Synthesis of isolated single-wall carbon nanotubes

Isolated, mainly single-wall carbon nanotubes were grown on TEM silicon nitride grids (DuraSiN DTM-25233) by chemical vapour deposition.[25] Catalyst particles were deposited on the substrate by drop casting a methanolic suspension of $Fe(NO_3)_3{\cdot}9H_2O$ (3.6 mM), $MoO_2(acac)_2$ (acac = acetylacetonate, 0.9 mM) and alumina nanoparticles (BET 85-115 $m^2.g^{-1}$, 1 $g.L^{-1}$) on the substrate. Single wall nanotubes were grown at 860°C[26] in a methane (0.52 $L.min^{-1}$) and dihydrogen (0.70 $L.min^{-1}$) flow for 10 min. The resulting material is of statistically mixed chirality.

Wet oxidation of bulk carbon nanotubes

A black suspension of single-wall carbon nanotubes (1.0 g) in an aqueous solution of nitric acid (7 M, 150 mL) was sonicated at 20°C for 10 min with a high frequency power output of 60 W and then refluxed for 6 hours. The carbon nanotubes were retrieved by centrifugation at 4000 rpm for 30 min, then thoroughly washed by sonicating in water (150 mL, ca. 1 min, HF power 120 W), then shaking the suspension for 1 h and centrifuging out again. The washing process was repeated three times in total. Oxidized amorphous carbon fragments were then removed by a basic wash:[27] The nanotubes were sonicated (30 min, 20°C, HF power 120 W) in a sodium hydroxide solution (0.01 M, 400 mL), then the suspension was shaken for 2 hours before the carbon nanotubes were collected by vacuum filtration on a PTFE filter (diameter 45 mm, pore diameter 0.45 µm). The base wash process was repeated until the filtrate, initially dark brown, became completely colourless (usually three to four times in total). The carbon nanotubes were sonicated (30 min, 20°C, HF power 120 W) then shaken (1 h) in an aqueous chlorhydric acid solution (0.01 M, 400 mL) to remove all traces of base, filtered out on a PTFE filter (diameter 45 mm, pore diameter 0.45 µm) and finally dried overnight under vacuum (0.85 g, 85 %).

Functionalization of oxidized carbon nanotubes with $\{Mn_4\}$

For bulk CNT functionalization, red microcrystalline $[Mn_4L_2(OAc)_4]$ (345 mg, 0.3 mmol) was added to a black suspension of oxidized carbon nanotubes (130 mg) in acetonitrile (30 mL) obtained by sonicating for 30 min (20°C, HF power 120 W). After shaking the suspension for a week, the nanotubes were collected by vacuum filtration on a PTFE membrane (diameter 45 mm, pore diameter 0.45 µm), quickly rinsed with acetonitrile (3×50 mL), resuspended in acetonitrile by sonicating for 30 min (20°C, HF power 120 W), filtered out and suspended again in fresh acetonitrile after three days of shaking, finally collected by filtration after four more days of shaking and dried under vacuum overnight. Increasing the reaction or washing time did not change the composition of the obtained product. TEM meshes with isolated CVD-grown nanotubes were fixed in a sample holder and introduced in an acetonitrile solution of $[Mn_4L_2(OAc)_4]$ (10 mM in acetonitrile, ca. 20 mL). After a week of reaction, the sample was carefully removed from the solution, gently rinsed with acetonitrile and introduced in acetonitrile (ca. 20 mL) for a week, with a change to fresh solvent after three days.

Results and discussion

Oxidation of the carbon nanotubes

Controlled oxidation introduces a large variety of defects on the extremities and sidewalls of carbon nanotubes. Carboxylic acid functions, in particular, have been extensively studied as an attractive entry point to carbon nanotube functionalization through electrostatic interaction (when deprotonated), amide bond or, more rarely, coordination to metal centres. Numerous oxidation methods for single-wall carbon nanotubes have been reported in the literature, yielding various ratios of carboxylic acid to other functions such as alcohols, lactones or anhydrides. For bulk samples designated for magnetometry experiments, we selected reflux in concentrated nitric acid, a procedure that presents the double advantage of eliminating the magnetic catalyst impurities present in the commercial nanotubes and providing a high concentration of carboxylic acid functions[28]. This oxidation method however is not suitable for the treatment of fragile samples such as isolated carbon nanotubes on a TEM grid; CNTs are removed from the substrate along with the catalyst.[29] On the long term, this technique would also most likely not be compatible with contacted nanotubes because the contacts may corrode. We therefore investigated the simpler oxidation of samples by heating at 450°C in air for 30 min, a process accompanied in bulk samples by a 15-25 % weight loss. Assuming the absence of elements other than C, H, N and O in the samples, CHN elemental analysis gives access to the compositions formulated in Table 1 indicating a doubling of the oxygen to carbon ratio following nitric acid

oxidation, while the air oxidation shows no notable effect on bulk samples. Raman spectroscopy and titration of the samples by sodium hydroxide confirm this trend. Nitric acid oxidation is accompanied by an increase of the D/G mode ratio in the Raman spectra as well as by an increase of the concentration of total acid functions from 0.5-1.0 mmol.g^{-1} to 2.0-2.7 mmol.g^{-1}, *i.e.* from 1.5-2.9 acidic functions per formula unit of $C_{218}H_{13}O_{17}$ before oxidation to 5.8-7.8 per formula unit of $C_{218}H_{39}N_2O_{35}$ after oxidation. After oxidation in air, however, the concentration of acidic functions is often stable or even reduced to 0.2-0.8 mmol.g^{-1} (2.5-10 acidic functions per $C_{959}H_{60}N_4O_{65}$), and the D/G mode ratio is mostly unchanged, probably because the creation of new defects is compensated by the elimination of any small polycyclic aromatic compounds present at the surface of the tube as well as by some degree of decomposition of the nanotube at existing defect sites, both phenomena accounting for the weight loss observed. In the case of carbon nanotubes grown on a substrate however, air oxidation is necessary to introduce defects in the initially almost pristine nanotubes, and the duration of the oxidation can be used to control the density of the defects.[24]

Table 1. Composition of bulk CNT samples.

Sample	Formula[a]
Commercial, as received	$C_{218}H_{13}O_{17} \equiv C_{959}H_{56}O_{65}$
After HNO_3 oxidation	$C_{218}H_{39}N_2O_{35}$
After HNO_3 oxidation and reaction with $[Mn_4L_2(OAc)_4]$	$C_{218}H_{38}N_2O_{35}$-{Mn_4}[b]
After air oxidation	$C_{959}H_{60}N_4O_{65}$[c]
After air oxidation and reaction with $[Mn_4L_2(OAc)_4]$	$C_{959}H_{59}N_4O_{65}$-{Mn_4}

[a]Based on an arbitrary number of carbon atoms. Values are ± 10 H, ± 1 N, ± 5 O; [b]{Mn_4} = $[Mn_4L_2(OAc)_3]^+$ (H_2L = 2,6-*bis*(1-(2-hydroxyphenyl)iminoethyl)pyridine); [c] The conditions of the oxidation reaction in air (temperature of 450°C, presence of alumina supported iron-based catalyst nanoparticles) are similar to those employed during the Haber-Bosch synthesis albeit at a much lower dinitrogen pressure (0.8 bar here vs. 200 bar in the industrial process). It is therefore likely that the small amount (ca. 0.4 % per weight) of nitrogen incorporated in the samples during this reaction results directly from activation of dinitrogen.[30]

Functionalization of the nanotubes

Introducing the oxidized carbon nanotubes in a solution of the complex $[Mn_4L_2(OAc)_4]$ at room temperature provides functionalized samples (Figure 1) following reaction

CNT-COOH + $[Mn_4L_2(OAc)_4]$ -> CNT-COO-$Mn_4L_2(OAc)_3$ + AcOH

Exhaustive washing of the material obtained ensures that complexes or fragments thereof that might be left adsorbed on the surface of the carbon nanotube are completely eliminated, leaving only chemically bound species. Manganese content, determined by ICP-OES elemental analysis or gravimetry of the Mn_2O_3 residue after decomposition in air at 700°C, ranges from 1.5 to 5 % per weight, increasing as the degree of oxidation of the carbon nanotube, and therefore the amount of carboxylic acid functions available for the reaction, increases. Additionally, Mn/N ratios are consistent with the expected ligand to metal stoichiometry, confirming the stability of the tetramanganese core upon functionalization. The obtained formulas are given in Table 1.

Stoichiometry varies from one tetramanganese complex per *ca.* 960 carbon atoms for air-oxidized samples to one complex per *ca.* 220 carbon atoms for nitric acid-oxidized samples, corresponding to coverage of the surface of the nanotubes with the complex from 6 % up to around 25 %. Assuming a diameter of 1 nm for the carbon nanotubes, this corresponds to one tetramanganese unit per 8 to 1.8 nm. While these results demonstrate the possibility of controlling the degree of functionalization of bulk carbon nanotubes, other techniques have to be employed to investigate isolated carbon nanotubes.

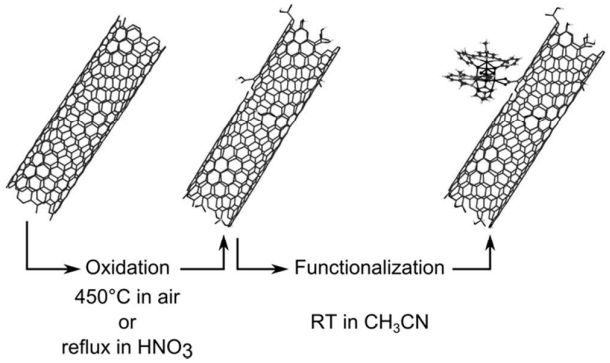

Fig. 1 Schematic representation of the carbon nanotube-tetramanganese complex.

Growing, air-oxidizing and functionalizing the carbon nanotubes directly on the TEM membrane allows for direct imaging of the obtained samples. A typical high-resolution TEM image of a low-density sample (Figure 2a) reveals a double-walled carbon nanotube with its hexagonal graphene lattice. Amorphous carbon is observed due to degradation of CNTs and decomposition of the ligands under the electron beam. Brighter sites (arrows) are characteristic of the presence of heavier atoms and thus indicate functionalization of the sites with tetramanganese complexes. The HAADF image of a CNT sample with similar low functionalization (t_{ox}= 2 min) is presented in the inset of Figure 2b. It reveals the heavy atom scattering centres more clearly due to the enhanced intensity with respect to the atomic number in HAADF mode (see more HAADF images of this sample in Figure S2).

EELS measurements taken on a scattering centre and on a supposedly not functionalized part of the CNT reveal that the scattering is indeed caused by Mn atoms (Figure 2b). Since the catalyst particles used for the synthesis of the CNTs contain Mo and Fe, these elements could act as scattering centres as well. However, no significant contribution of these elements is present in the EELS measurements (compare Figure 2b).

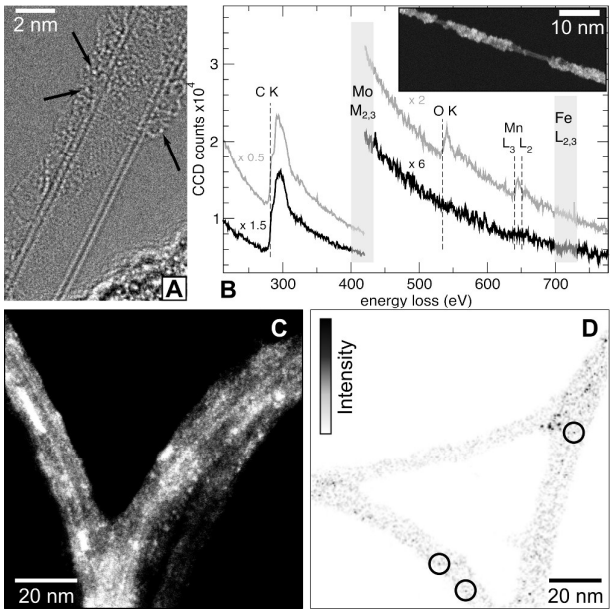

Figure 2. a) Bright-field HR-TEM image of low-functionalization (t_{ox} = 3 min) carbon nanotube. Exceptionally bright spots (arrows) indicate the presence of manganese atoms. The electron beam leads to partial degradation of the CNTs during the measurement. b) Local EELS measurements using STEM of a low-functionalization sample (t_{ox} = 2 min, HAADF inset). The top curve, showing a manganese signal, corresponds to the brighter parts on the tube, while the bottom curve corresponds to darker parts of the tube. Shaded areas indicate expected peak positions of the heavy elements present in the catalyst c) HAADF image of a sample with high functionalization (t_{ox} = 30 min). d) Bright field, energy-filtered TEM of the sample shown in a) (different position) taken at the Mn *L*-edge. Individual Mn atoms exemplary marked by black circles. Agglomeration of Mn clusters is due to electron beam induced mobility of the Mn atoms observed during imaging.

In Figure S1 of the supporting information we show a direct correspondence between HAADF and EELS data. Longer oxidation times preceding the functionalization, which are known to increase the number of defects created,[24] also lead to a stronger coverage of the CNTs with Mn as shown in Figure 2c. EDX spectra of this sample reveal no significant contribution of elements from the catalyst particles, either (compare Figure S3 of the supporting information), thus the scattering centres are predominantly Mn atoms. This is also in accordance with the results reported above for bulk samples that show larger Mn content with increasing oxidation.

Higher spatial resolution of the Mn distribution (~ 1 nm) in a low-density functionalized sample (t_{ox} = 3 min) is obtained using energy-filtered imaging in bright field integrating over the Mn *L*-edge (Figure 2d). Mn atoms are found to be on well-isolated positions, three of them exemplarily marked by the black circles. The distance between them can be as large as several tens of nanometres. Nanoelectronic transport devices can easily be scaled down to structure sizes below 40 nm. Therefore, it appears feasible to fabricate devices from similarly prepared CNT-tetramanganese assemblies that contain only few complexes or even just a single one.

Magnetic characterization

Charge transfer is sometimes observed between metallic complexes and the carbon nanotubes they are attached to.[31] Such a process has the potential to significantly alter the magnetic properties of the assembly, and in particular to modify the desired diamagnetic ground state of the molecule. The preservation of the magnetic properties of the tetramanganese cluster after attachment to nitric acid-oxidized carbon nanotubes was investigated by SQUID magnetometry. The magnetic moment per tetramanganese fragment was calculated from the experimental data using the formula obtained in Table 1. A small residual contribution due to the carbon nanotube was measured on a non-functionalized sample and subtracted from the data before further analysis.

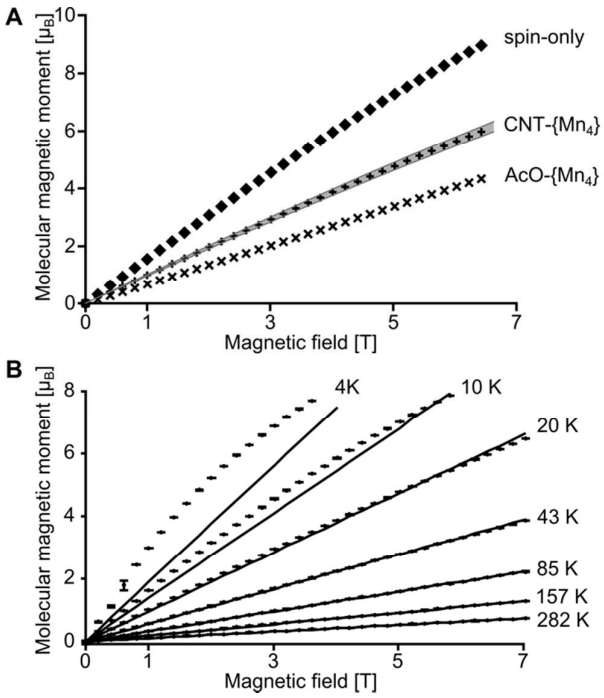

Fig. 3 a) SQUID magnetometry data (T = 20 K) of $[Mn_4L_2(OAc)_4]$ (**X**), typical CNT-$[Mn_4L_2(OAc)_3]$ (**+**) (confidence interval represents the variations due to imprecision in the measurement of the manganese contents for the specific sample considered) and calculated, spin-only Mn^{II}_4 (◆). b) Complete temperature-dependent (4 to 282 K) magnetization data for CNT-$[Mn_4L_2(OAc)_3]$ (error bars are standard deviations due to SQUID measurement only) and Curie-Weiss model (plain line) obtained by fitting the data above 40 K.

Comparison of the temperature-dependent magnetization curves of the tetramanganese complex before and after attachment to the carbon nanotube (Figure 3a) indicates that the coupling within the bound tetramanganese unit remains predominantly antiferromagnetic as desired. However, the amplitude of the coupling is altered, as can be expected

considering the change of one of the bridging ligands from acetate to nanotube-bound carboxylate. A Curie-Weiss (mean field approximation) fit of the data for temperatures above 40 K (Figure 3b) give a Curie constant $C_{CNT\text{-}\{Mn4\}} = 0.0031\ m^3.K.mol^{-1}$ in agreement with the value expected for four $S = 5/2$ Mn^{II} centres and a Weiss temperature $\vartheta_{CNT\text{-}\{Mn4\}} = -13$ K (corresponding to a sum of coupling values of *ca.* -1.5 cm^{-1} using $H_{ab} = -2J_{ab}S_aS_b$). Below 40 K the simple Curie-Weiss model is not sufficient to account for the complex interaction between the four Mn ions. The values obtained for the same Curie-Weiss fit of the free $[Mn_4L_2(OAc)_4]$ complex data are $C_{\{Mn4\}} = 0.0030\ m^3.K.mol^{-1}$ and $\vartheta_{\{Mn4\}} = -23$ K (coupling values of -2.7 cm^{-1}). This indicates a weakening of the antiferromagnetic interactions within the complex upon attachment to the tube. Interestingly, Curie-Weiss fits conducted on the data published by Rowan *et al.* on the benzoate and trifluoroacetate analogues $[Mn_4L_2A_4]$ ($A = PhCOO^-$, CF_3COO^-) give Weiss temperatures of -17 K and -7 K respectively, corresponding to a weakening of the antiferromagnetic coupling which was attributed to the electron withdrawing effects of the phenyl and trifluoromethyl groups compared to the methyl group in the acetate derivative. This is in good agreement with the known electron acceptor characteristics of carbon nanotubes.[32]

Conclusions

In this communication, we demonstrate the coordination of well-defined, polynuclear complexes to oxidized carbon nanotubes by a short, direct, and rigid bond. The interaction with the nanotube causes a weakening of the predominantly antiferromagnetic coupling between the ions but does not fundamentally alter the magnetic properties. Density control of the functionalization is obtained by different means of oxidation and oxidation time. For short oxidation time $t_{ox} \leq 3$ min, the coverage of the tube with $\{Mn_4\}$ becomes so low that the distance between two complexes can reach several tens of nanometres. Therefore, field effect transistors can be fabricated from these CNTs with only a single molecule attached. The interaction between spin states of such a molecule with the spins of the conduction electrons of a CNT can then be detected in electric transport measurements.

Acknowledgements

We thank Cate Morgan for help with the SQUID measurements. Funding from DFG (FOR912) and JARA-FIT Seed fund is acknowledged.

References

1 Y. Choi, I. S. Moody, P. C. Sims, S. R. Hunt, B. L. Corso, I. Perez, G. A. Weiss and P. G. Collins, *Science*, 2012, **335**, 319-324.
2 Y. Zhao, B. Ashcroft, P. Zhang, H. Liu, S. Sen, W. Song, J. Im, B. Gyarfas, S. Manna, S. Biswas, C. Borges and S. Lindsay, *Nat. Nanotechnol.*, 2014, **9**, 466-473.
3 M. L. Perrin, R. Frisenda, M. Koole, J. S. Seldenthuis, A. C. GilJose, H. Valkenier, J. C. Hummelen, N. Renaud, F. C. Grozema, J. M. Thijssen, D. Dulic and H. S. J. van der Zant, *Nat. Nanotechnol.*, 2014, **9**, 830-834.
4 I. Willner, B. Basnar and B. Willner, *Adv. Funct. Mater.*, 2007, **17**, 702-717.
5 D. Xiang, H. Jeong, D. Kim, T. Lee, Y. Cheng, Q. Wang and D. Mayer, Nano Lett., 2013, **13**, 2809-2813.
6 E. A. Osorio, K. Moth-Poulsen, H. S. J. van der Zant, J. Paaske, P. Hedegråd, K. Flensberg, J. Bendix and T. Bjørnholm, Nano Lett., 2009, **10**, 105-110.
7 J. Lehmann, A. Gaita-Arino, E. Coronado and D. Loss, *Nat. Nanotechnol.*, 2007, **2**, 312-317.
8 J. Lehmann, A. Gaita-Arino, E. Coronado and D. Loss, *J. Mater. Chem.*, 2009, **19**, 1672-1677.
9 M. N. Leuenberger and D. Loss, *Nature*, 2001, **410**, 789-793.
10 S. Thiele, F. Balestro, R. Ballou, S. Klyatskaya, M. Ruben and W. Wernsdorfer, *Science*, 2014, **344**, 1135-1138.
11 E. A. Osorio, T. Bjørnholm, J. M. Lehn, M. Ruben and H. S. J. v. d. Zant, *J. Phys. Condens. Matter*, 2008, **20**, 374121.
12 M. Ratner, *Nat. Nanotechnol.*, 2013, **8**, 378-381.
13 L. Bogani, R. Maurand, L. Marty, C. Sangregorio, C. Altavilla and W. Wernsdorfer, *J. Mater. Chem.*, 2010, **20**, 2099-2107.
14 L. Bogani and W. Wernsdorfer, *Nat. Mater.*, 2008, **7**, 179-186.
15 B. I. K. Kharisov, O. V., *J. Coord. Chem.*, 2014, **67**, 3769-3808.
16 E. V. V. Rybak-Akimova, O.E. ; Wikstrom, J., in *Chemistry of Carbon Nanotubes*, ed. V. A. B. Basiuk, E. V., Los Angeles, CA, American Scientific Publishers, 2008, vol. 2, ch. 18, pp. 82-108.
17 D. Tasis, N. Tagmatarchis, A. Bianco and M. Prato, *Chem. Rev.*, 2006, **106**, 1105-1136.
18 G. Gavrel, B. Jousselme, A. Filoramo and S. Campidelli, in *Making and Exploiting Fullerenes, Graphene, and Carbon Nanotubes*, eds. M. Marcaccio and F. Paolucci, Springer Berlin Heidelberg, 2014, vol. 348, ch. 450, pp. 95-126.
19 B. Jousselme, A. Filoramo and S. Campidelli, in *Supramolecular Chemistry of Fullerenes and Carbon Nanotubes*, Wiley-VCH Verlag GmbH & Co. KGaA, 2012, DOI: 10.1002/9783527650125.ch11, pp. 263-300.
20 C. Bosch-Navarro, E. Coronado, C. Martí-Gastaldo, B. Rodríguez-González and L. M. Liz-Marzán, *Adv. Funct. Mater.*, 2012, **22**, 979-988.
21 S. Banerjee, T. Hemraj-Benny and S. S. Wong, *Adv. Mater.*, 2005, **17**, 17-29.
22 F. Hauke and A. Hirsch, in *Carbon Nanotubes and Related Structures*, Wiley-VCH Verlag GmbH & Co. KGaA, 2010, DOI: 10.1002/9783527629930.ch6, pp. 135-198.
23 E. Kampert, F. F. B. J. Janssen, D. W. Boukhvalov, J. C. Russcher, J. M. M. Smits, R. de Gelder, B. de Bruin, P. C. M. Christianen, U. Zeitler, M. I. Katsnelson, J. C. Maan and A. E. Rowan, *Inorg. Chem.*, 2009, **48**, 11903-11908.
24 C. Meyer, C. Besson, R. Frielinghaus, A.-K. Saelhoff, H. Flötotto, L. Houben, P. Kögerler and C. M. Schneider, *Phys. Status Solidi B*, 2012, **249**, 2412-2415.
25 J. Kong, H. T. Soh, A. M. Cassell, C. F. Quate and H. Dai, *Nature*, 1998, **395**, 878-881.
26 C. Spudat, C. Meyer, K. Goss and C. M. Schneider, *Phys. Status Solidi B*, 2009, **246**, 2498-2501.

27 K. A. Worsley, I. Kalinina, E. Bekyarova and R. C. Haddon, *J. Amer. Chem. Soc.*, 2009, **131**, 18153-18158.

28 I. Gerber, M. Oubenali, R. Bacsa, J. Durand, A. Gonçalves, M. F. R. Pereira, F. Jolibois, L. Perrin, R. Poteau and P. Serp, *Chem. Eur. J.*, 2011, **17**, 11467-11477.

29 C. Meyer, C. Spudat, L. Houben and C. M. Schneider, *Nanotechnology*, 2009, **20**, 065603.

30 Eggeman, T. 2010, Ammonia. Kirk-Othmer Encyclopedia of Chemical Technology. 1–33.

31 C. Oelsner, M. A. Herrero, C. Ehli, M. Prato and D. M. Guldi, *J. Amer. Chem. Soc.*, 2011, **133**, 18696-18706.

32 F. Buonocore, F. Trani, D. Ninno, A. D. Matteo, G. Cantele and G. Iadonisi, *Nanotechnology*, 2008, **19**, 025711.